JOURNAL OF MATERIALS SCIENCE **38** (2003) 4271–4282

Oxygen sensors: Materials, methods, designs and applications

R. RAMAMOORTHY*, P. K. DUTTA‡, S. A. AKBAR
Center for Industrial Sensors and Measurements (CISM), Department of Materials Science and Engineering, The Ohio State University, 2041 College Road, Columbus, OH 43210, USA
E-mail: ramasamy@mse.eng.ohio-state.edu

Advancement of gas sensor technology over the past few decades has led to significant progress in pollution control and thereby, to environmental protection. An excellent example is the control of automobile exhaust emissions, made possible by the use of oxygen gas sensors. Since early 1970's there have been sustained studies on oxygen sensors and has led to development of sensors for various applications with varying performance characteristics. Solid electrolyte based potentiometric, amperometric and metal oxide based semiconducting resistive type sensors are used for high temperature applications. For solution-based pollution monitoring, dissolved oxygen sensors based on Clark electrodes have played a major role. More recently, for biological and medical applications, optical oxygen sensors are beginning to have an impact. In this review, we focus on both high temperature as well as dissolved oxygen sensors and compare the different methods of oxygen sensing, discuss underlying principles, and outline the designs and specific applications.

1. Introduction

Concern over environmental pollution and health issues has driven legislation over the past two decades and significant research and development efforts have been undertaken to address environmental issues. Worldwide research in the field of gas sensors for many years has been driven by the desire to minimize emissions from various industrial sources [1–4]. In particular, oxygen sensors have played a key role in pollution control through automobile engine management, optimizing industrial boilers, steel, cement industries, biological and food processing plants and control of chemical processes [5]. Based on the number of sensors in operation, the predominant use of oxygen sensors is in the control of air-fuel mixture in the combustion engine of the automobiles and is an integral part of the 'on board diagnostic' (OBD) of the exhaust emission control system [6, 7].

The concentration or the partial pressure of oxygen in an environment can be determined using different measuring principles. For high temperature measurements of oxygen, ceramic-based sensors are the most practical. Equilibrium potential measurements on solid electrolyte-electrode cells enable oxygen measurement via the Nernst equation. Sensors of this kind are called potentiometric sensors and the sensor output varies logarithmically with oxygen partial pressure. These sensors provide reproducible, stable and accurate measurements of even low levels (ppm) of oxygen. By imposing a diffusion barrier between the test gas flow and the electrode, the electrolyte-electrode cell can be operated in the polarographic mode. Then the current flowing through the cell provides a measure of oxygen, and is called limiting current amperometric sensor. As such, this sensor does not require reference oxygen column and can respond linearly with oxygen concentration. Semiconductor based sensors measure oxygen via changes in electrical conductance arising from alteration of the defect chemistry by chemisorption of oxygen. All of the sensors described above operate at high temperatures ranging from 300 to 1000°C and can be used in harsh environments.

Monitoring oxygen under ambient conditions and especially as dissolved oxygen is necessary in medical, food processing and waste management industries. The sensors that are used for such applications include Clark electrodes, aqueous electrochemical cells, paramagnetic gas sensors and optical sensors [3, 5].

A working sensor is typically characterized by three parameters: sensitivity, selectivity and response time. Sensitivity is the ability of the sensor to quantitatively measure the test gas under given conditions. It is governed by the inherent physical and chemical properties of the materials used. Selectivity of a sensor is its ability to sense a particular gas free from interference. Response time is a measure of how quickly the maximum signal change is achieved with gas concentration changes. In addition, reversibility, long term stability, size, and power consumption are other factors influencing the overall performance of the sensor.

*Author to whom all correspondence should be addressed.
‡*Present address*: Department of Chemistry, The Ohio State University, 120 W 18th Avenue, Columbus, Ohio 43210, USA.

In this review, we discuss the principles behind oxygen measurements at high temperatures and under ambient conditions. Equilibrium potentiometric, limiting current amperometric and semiconducting sensors form the topic of high temperature applications and optical sensors are discussed from the viewpoint of ambient oxygen sensing.

2. High temperature sensors

2.1. Potentiometric equilibrium sensors

Solid state potentiometric oxygen sensors typically use an oxygen ion conducting material as electrolyte. Many solid electrolytes with reasonable electrical conductivities have been studied and Table I provides a partial list [8–11]. Amongst these, yttria stabilized zirconia (YSZ) has been the material of choice [12, 13] due to its ionic nature and better stability in harsh environments. In the case of YSZ, oxygen ion transport is due to the movement of oxygen ion vacancies created by doping yttria in zirconia. A doping level of 6–12 mol% of yttria stabilizes zirconia in the cubic phase, a more favorable phase for ionic conduction at high temperatures [14]. The oxygen stoichiometry, crystal structure, mechanical and electrical properties of YSZ are stable over a large temperature ranging from room temperature up to its softening point (~2500°C).

Fig. 1 shows a schematic diagram of a thimble type YSZ based oxygen sensor. The output of this potentiometric sensor is due to the combined effect of chemical and electrical processes. When the sensor is exposed to a test gas environment, the oxygen molecules get adsorbed onto the porous electrode, commonly made of platinum, and dissociate into atomic oxygen. Then the oxygen atoms diffuse into the boundary of the electrode (Pt), electrolyte (YSZ) and the gas called the 'triple phase boundary'(TPB), where electron transfer takes place from the electrode to the atomic oxygen forming O^{2-} ions (reduction). The overall electrode reactions are as follows [15, 16]:

$$O_{2_{ads(Pt)}} \rightarrow O_{ads(Pt)} + O_{ads(Pt)} \rightarrow O^{2-}_{TPB} \rightarrow O^{x}_{YSZ} \quad (1)$$

All the reaction steps in Equation 1 can be represented in a simpler form as

$$\frac{1}{2}O_{2(g)} + 2e^{-}_{(Pt)} + V_{O(YSZ)} \rightleftharpoons O^{x}_{YSZ} \quad (2)$$

In order to facilitate processes involved in Equation 1, the electrode needs to be a good catalyst for oxygen reduction and oxidation. The electrode microstructure needs to be porous to manifest enough triple phase boundaries and the electrolyte needs to be a good oxygen ion conductor at the operating temperature of the device. The presence of gaseous oxygen at the electrode-electrolyte interface defines a value for oxygen activity and the Fermi level (E_F) is controlled at the interface by the oxygen-electrode equilibrium [17]

$$O_{2(gas)} + 4e^{-}_{(electrode)} \rightleftharpoons 2O^{2-}_{(electrolyte)} \quad (3)$$

$$E_F = \frac{1}{4}\left(2\mu_{O^{2-}} - \mu_{O_2}\right) \quad (4)$$

where μ is the chemical potential. Since YSZ is a good oxide ion conductor and has high vacancy concentration (proportional to the mole fraction of the dopant yttria), the chemical potential of oxide ions within the YSZ electrolyte is unchanged. So, for different partial pressures of oxygen P'_{O_2} and P''_{O_2} on two sides, the difference in Fermi levels is given by

$$\Delta E_F = -\frac{1}{4}\left(\mu'_{O_2} - \mu''_{O_2}\right) = -\frac{kT}{4e}\ln\left(P'_{O_2}/P''_{O_2}\right) \quad (5)$$

Thus, the potential difference (emf) measured between the two electrodes is given by

$$\text{emf} = \frac{RT}{4F}\ln\left(\frac{P'_{O_2}}{P''_{O_2}}\right) \quad (6)$$

where F is the Faraday constant. Equation 6 is the Nernst eq. for the electrochemical cells. The sensitivity of the equilibrium potentiometric sensors is given by $RT/4F$ and depends only on temperature, provided the electrolyte is a pure ionic conductor. On the other hand, the response time is influenced by rate constants involved in Equation 1. The slowest process will be the rate determining step for the response time of the sensor. Fig. 2 shows a typical response curve of a potentiometric oxygen sensor. The sensor output depends logarithmically on P_{O_2} as shown in the inset of Fig. 2.

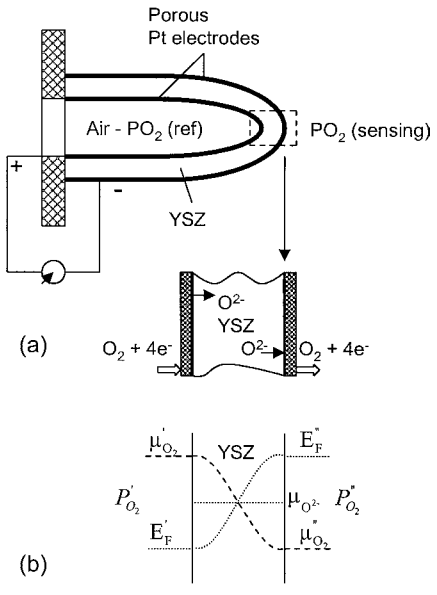

Figure 1 Schematic diagram of a potentiometric oxygen sensor employing a thimble YSZ electrolyte and platinum electrodes (a) and the chemical potential profile in the sensor cell (b).

TABLE I Electrical conductivity values of solid oxide electrolytes at 600°C

Oxygen ion conducting solid electrolytes[a]	Conductivity ($S\ cm^{-1}$)	Ref.
Bi_2O_3	3×10^{-3}	[8]
Gd_2O_3 doped CeO_2	4×10^{-3}	[9]
$Bi_2Cu_{0.1}V_{0.9}O_{5.35}$	1×10^{-1}	[10]
YSZ (8 mol% Y_2O_3)	5×10^{-2}	[11]

[a]Other than YSZ, all the electrolytes possess certain level of electronic conductivity as well.

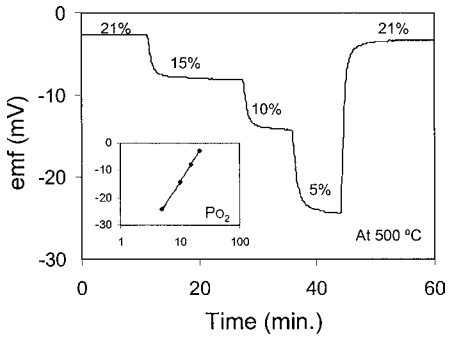

Figure 2 Typical sensor response curve of a thimble type YSZ based potentiometric oxygen sensor. Inset: semi-logarithmic variation of the sensor output with P_{O_2}.

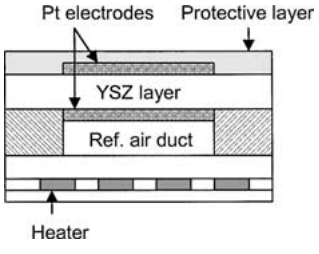

Figure 3 Cross sectional view of a planar oxygen sensor [18].

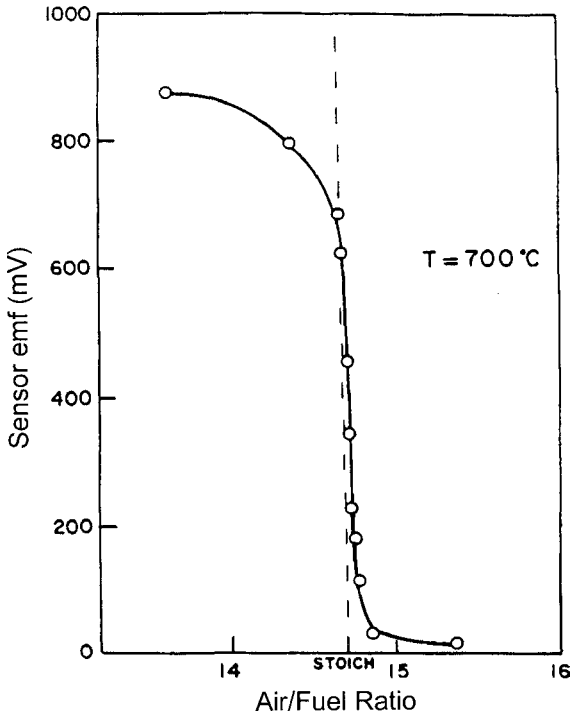

Figure 4 Typical response of a commercial ZrO_2 oxygen sensor to changes in A/F of an engine [22].

The slope of the Nernstian line, the sensitivity of the sensor, can be increased by increasing the operating temperature of the sensor device.

In 1976, Bosch introduced a YSZ-based thimble type oxygen sensor to control the air-to-fuel ratio in automobile engines [18]. This unheated O_2 sensor relied on the exhaust gases to reach the operating temperature and therefore an interval of time was required before optimum sensor functioning. On the other hand, planar sensor elements show faster response characteristics due to reduced size and thermal mass. Planar oxygen sensor is based on the tape-cast or thick film technology. Fig. 3 shows the cross sectional view of a planar O_2 sensor design. The active layers of such a sensor, the base substrate, heater, reference air-duct, electrodes, and the sensing element, are stacked together in the green state and laminated by high temperature treatments [7, 18]. This layer configuration enables integration of the heating element within the sensor body itself. The low thermal mass and reduced size of the sensing element (YSZ layer) and the integrated heater allows for fast response and therefore, better control over the emissions during the engine start-up. Further developments in the O_2 sensor designs involve fabrication of reference-air free potentiometric oxygen sensors making use of non-stoichiometric metal oxides, e.g., Ni-NiO solid mixture [19–21].

The main application of oxygen sensors in the gasoline run automobiles is to control the air-to-fuel ratio (λ). Table II lists the types of oxygen sensors used in automobiles. The oxygen partial pressure changes abruptly in the vicinity of the stoichiometric mixture of the air and the fuel ($\lambda = 1$: air = 14.5 kg; fuel = 1 kg) [13]. Fig. 4 shows the characteristic sensor output, the λ-curve, for a range of air-fuel mixture in the combustion engine [22]. The emissions of toxic gases such as CO, NO_x, and hydrocarbons (HC) depend on the λ point at which the engine functions. In the fuel rich region, the emission of CO and HC dominates and in the lean region, NO_x emission is larger [6]. These exhaust gases are converted to non-toxic gases CO_2, N_2, and H_2O by a three way catalytic converter located in the exhaust system. The O_2 sensor output is fed back to the engine control so that the engine operates between the rich and lean fuel conditions centered around the stoichiometric ratio. However, during the cold start of the engine, the feed back signal from the O_2 sensor is quite arbitrary

TABLE II Materials, applications and limitations of different types of oxygen sensors

Sensor type	Materials used in sensors	Principle	Applications	Limitations
Potentiometric	YSZ	Nernst principle	As λ-sensor in automobiles; combustion monitoring in industrial boilers, etc.	Output signal varies logarithmically with P_{O_2}; not suitable for lean burn engine
Amperometric	YSZ	Polarographic oxygen pumping	Wide range O_2 sensor in automobiles	More complicated packaging and design; complexity in diffusion barrier control
Resistive semiconductor	TiO_2	Defects induced conductance variation	As λ-sensor in automobiles	Base resistance drift with time

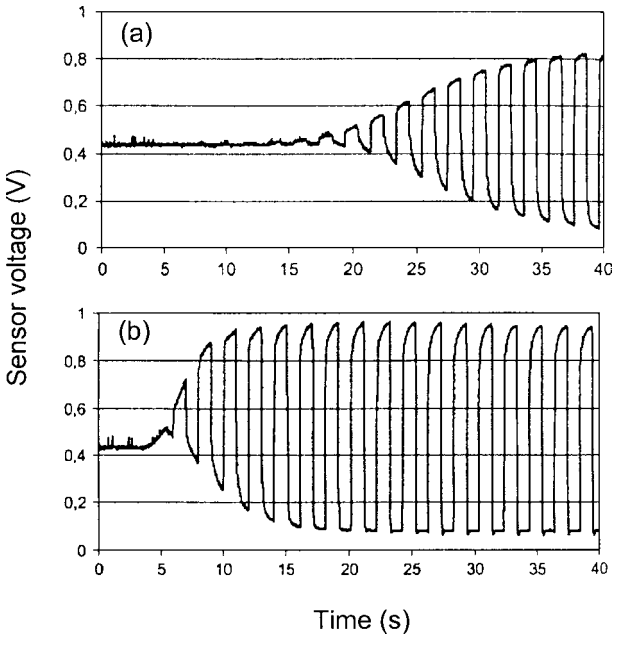

Figure 5 Typical light off time behaviors of ZrO_2 oxygen sensors: (a) heated thimble type and (b) heater integrated planar type sensing elements [7].

until it reaches the required temperature of operation. This light-off time has been reduced from minutes to a few seconds by implementing design changes. Fig. 5 compares typical light-off times for thimble type and planar O_2 sensors [7].

The above described potentiometric thimble type and planar O_2 sensors are only meant to work around stoichiometric air to fuel ratio ($\lambda = 1$). To improve fuel economy, a possible strategy is to run the engine in fuel lean conditions. Under appropriate fuel lean conditions (e.g., 18:1 or 22:1 air to fuel), a compromise can be reached between the engine power output, emission of green house gases and fuel economy [13]. In these situations, the engine control demands a direct and linear measurement of oxygen in the system. For such applications, solid state amperometric sensors based on YSZ electrolyte have been devised.

2.2. Limiting current amperometric sensor

In the amperometric sensing mode, oxygen is pumped from one side of the electrolyte to the other by the application of an external potential to the cell. The resulting ionic current flowing through the electrolyte is a function of the oxygen concentration. The amperometric gas sensing mechanism is well known for measuring dissolved oxygen in liquids [23]. The diffusion coefficient of dissolved oxygen in aqueous solutions is four or five orders of magnitude lower than that for oxygen in the gas phase (150 $mm^2\ s^{-1}$ at 700°C). The high diffusion coefficient of gaseous oxygen results in an increase of the ionic current through the electrolyte with applied potential until break down occurs and no limiting current is observed. In order to limit the current for a given concentration of oxygen, a diffusion barrier for oxygen is introduced ahead of the cathode. The diffusion barrier can either be a small aperture or a porous

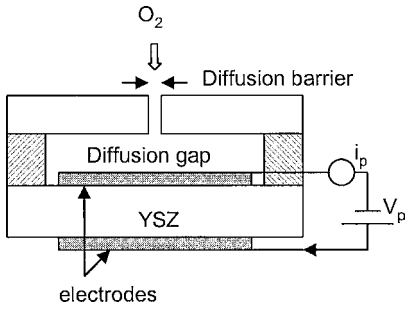

Figure 6 A current limiting diffusion barrier amperometric oxygen sensor based on YSZ electrolyte.

material on top of the cathode. Fig. 6 shows a cross sectional view of an amperometric sensor based on the YSZ electrolyte.

The gas sensing mechanism is controlled by the diffusion of oxygen and can be bulk or Knudsen diffusion process depending on the dimensions of the aperture. If the diameter 'd' of the diffusion hole is bigger than the mean free path 'ℓ' (i.e., the Knudsen number, $\mathrm{Kn} = \ell/d \ll 1$), then the rate determining step is gas-gas collisions rather than gas-wall collisions. This is the case of bulk diffusion. On the other hand, if $d \ll \ell$, i.e., $\mathrm{Kn} \gg 1$, then the gas-wall collisions are dominant and the diffusion process is called Knudsen diffusion. The current-voltage characteristics and hence the sensor properties are quite different between bulk and Knudsen diffusion, and thus, the limiting current is a function of the geometrical parameters of the diffusion barrier [24]. A detailed study by Usui *et al.* [25, 26] has shown that the limiting current varies with the oxygen concentration (C_{O_2}) as $-\ln(1 - C_{O_2})$ in bulk diffusion and linearly with C_{O_2} in Knudsen diffusion. Also it is interesting to note that the aperture of diameter about 20–30 μm showed both bulk and Knudsen diffusion of oxygen for the total pressure above and below 0.4 atm, respectively. For the total pressure of 1×10^{-3} atm (1 mm Hg), the Knudsen diffusion process dominates and the limiting current is directly proportional to the oxygen concentration. The current-voltage characteristics of a limiting current amperometric oxygen sensor in the Knudsen diffusion condition and the relationship between the limiting current and the oxygen concentration at low pressures are shown in Fig. 7a and b, respectively [26].

For a linearly varying limiting current sensor, the diffusion aperture must obey the criterion $\mathrm{Kn} \gg 1$, for a given range of the total pressure. In such a case, the diffusion current of molecular oxygen $\mathrm{d}N_{O_2}/\mathrm{d}t$ depends on the concentration gradient of oxygen $\mathrm{d}C_{O_2}/\mathrm{d}x$, the effective diffusion cross section Q and the diffusion coefficient of oxygen D_{O_2} and given by [18]

$$\frac{\mathrm{d}N_{O_2}}{\mathrm{d}t} = -D_{O_2} Q \frac{\mathrm{d}C_{O_2}}{\mathrm{d}x} \tag{7}$$

And the pumping ionic current flowing through the electrolyte cell is given by the Faraday's law

$$i_p = 4F \frac{\mathrm{d}N_{O_2}}{\mathrm{d}t} \tag{8}$$

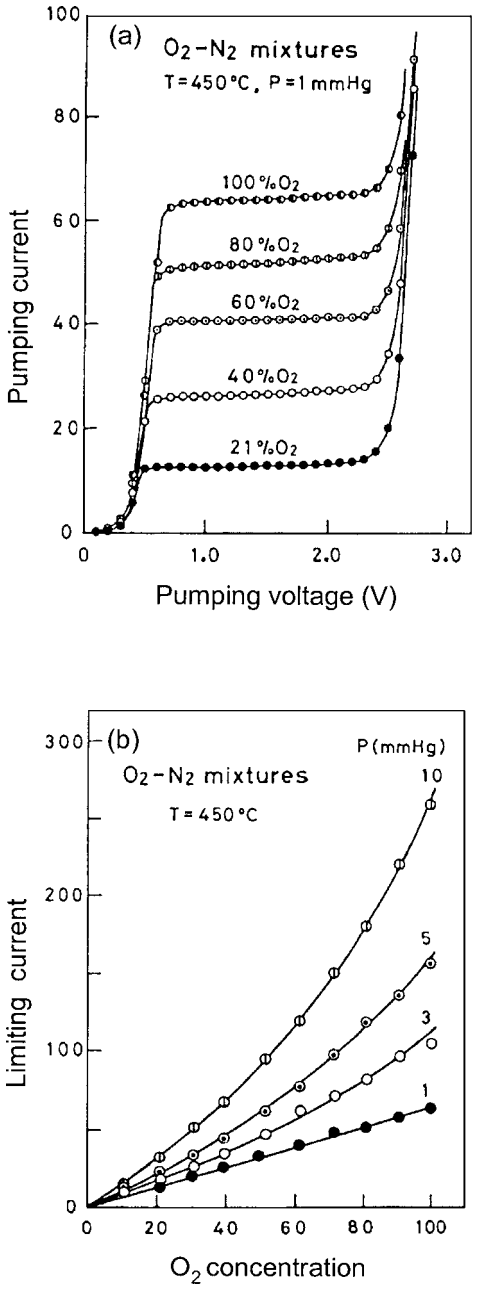

Figure 7 Limiting current-voltage characteristics of an amperometric oxygen sensor for varying: (a) pumping voltage and oxygen concentration and (b) oxygen concentration and total pressure [26].

As the applied pumping voltage V_p is increased, the current also increases until the oxygen pressure near the cathode-electrolyte interface reaches a value near zero. Then the current saturates at a value depending on the molecular current of the oxygen flow along the diffusion barrier. Now the limiting current i_p is directly proportional to the oxygen concentration in the test gas and linearly varying. As can be seen in Fig. 7a, the lowest applied potential in the limiting current region is around 500–600 mV and that is the usual pumping voltage in most of the sensors of this kind.

As mentioned earlier, the amperometric oxygen sensors were devised for the operation under lean fuel ($\lambda > 1$) conditions in the combustion systems. But the disadvantage is that if the combustion region is switched from lean to rich ($\lambda \leq 1$), the anode which is exposed to fuel mixture experiences a potential change of about 500 mV. Then the applied voltage needs to be increased to more than 1 V for the limiting current to flow, and is enough to drive the reduction of CO_2 and H_2O at the cathode, causing erroneous i_p values. The limiting current increases again for decrease of λ from the stoichiometric value of $\lambda = 1$ [27, 28] as shown in Fig. 8 [29]. So, for the observed value of the i_p, whether the combustion engine is operating under lean or rich region is unknown.

To overcome this problem, a two stage cell design has been developed: a pumping cell and a gauge cell or Nernst cell. In this sensor design, an internal diffusion gap volume is enclosed by the pumping and sensing (Nernst) YSZ elements and a porous material acts as the diffusion barrier. The sensing cell operates in the potentiometric mode and the output emf given by Equation 6 is used to control the pumping current by using a closed loop electronic circuit as shown in Fig. 9 [7, 18]. This feedback circuit enables the Nernst cell keep the oxygen partial pressure in the internal diffusion gap constant always around the stoichiometric mixture of the air and fuel ($\lambda = 1$). Thus, depending on the polarity of the pumping voltage, oxygen can either be pumped out or into the diffusion gap volume. In the steady state, the oxygen flux pumped out of the diffusion gap is equal to the flux of oxygen leaking through the diffusion barrier into the gap and hence creates a constant P_{O_2} in that gap. In this condition

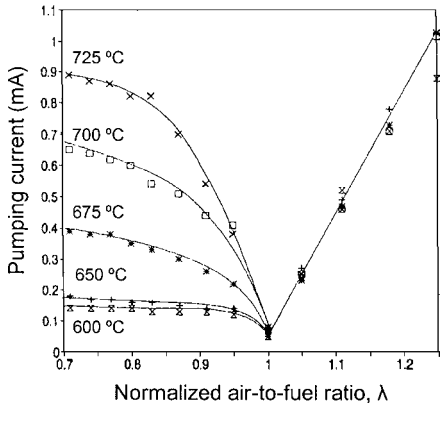

Figure 8 Characteristics of an amperometric sensor in the flue of a combustion system burning natural gas in air [29].

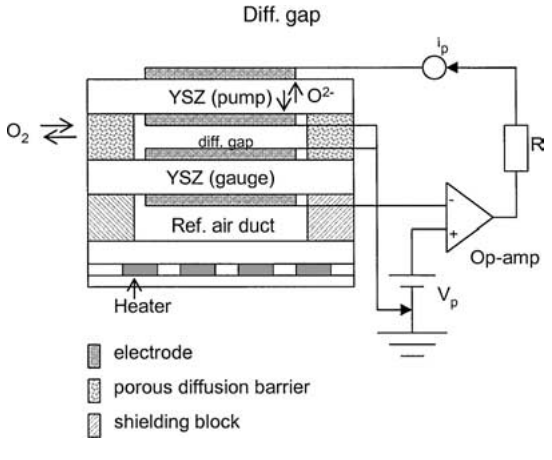

Figure 9 A dual cell, gauge and pumping, limiting current amperometric wide range oxygen sensor [7].

[28, 30],

$$\frac{i_p}{4F} = \sigma_{O_2}\left(P_{O_2} - P_{O_{2,d}}\right) \quad (9)$$

where P_{O_2} and $P_{O_{2,d}}$ are the partial pressures of oxygen in the outer ambient and the internal diffusion gap, respectively. σ_{O_2} is the leak conductance of O_2 along the diffusion barrier. For given geometrical parameters of the diffusion barrier,

$$\sigma_{O_2} = \frac{D_{O_2} A}{RTl} \quad (10)$$

where D_{O_2} is the diffusion coefficient of oxygen, A and l are the effective area of cross section and length of the diffusion barrier, respectively. By connecting the inner electrodes of the pumping and the Nernst cells in the diffusion gap volume to a short circuit, a uniform pressure of oxygen between those electrodes, $P_{O_{2,d}}$, can be expected and can be measured by the Nernst cell according to Equation 6

$$V_s = \frac{RT}{4F} \ln\left(\frac{P_{O_2}}{P_{O_{2,d}}}\right) \quad (11)$$

$$i_p = 4F\sigma_{O_2} P_{O_2}\left[1 - \exp\left(-\frac{4FV_s}{RT}\right)\right] \quad (12)$$

where V_s is the Nernst cell voltage (emf). From this equation, it is clear that for a given temperature, if V_s is constant, the pumping current is directly proportional to the product of σ_{O_2} and P_{O_2} for the full range of λ values from rich to lean region in the combustion system.

The electronic feedback circuit, making use of an operational amplifier (op-amp) in the differential mode, controls the pumping voltage polarity and hence the direction of current flow through the pumping cell which in turn provides a constant oxygen concentration in the internal diffusion gap and thus a constant V_s is established throughout the sensing process. When the combustion engine runs in the lean fuel region, the oxygen rich exhaust gas diffuses into the diffusion gap and the output of the Nernst cell and drives the circuitry so that oxygen is pumped out from the diffusion gap and λ reaches the stoichiometric value ($\lambda = 1$). If the ambient is at the stoichiometric value of λ, no current flows through the pumping cell. When the ambient corresponds to fuel rich condition, the Nernst emf drives the circuitry in the reverse direction causing the cell to pump oxygen into the diffusion gap adjusting the $P_{O_{2,d}}$ to a value near $\lambda = 1$. Thus there is a continuous change in the pumping current from positive to negative value as the combustion engine switches from lean to rich region as shown in Fig. 10. Thus the dual chamber pump—gauge amperometric sensor with air reference measures directly the oxygen concentration in the exhaust gases and the control over the combustion process is made accurately for a wide range of λ values. The thick film technology with integrated heater makes these sensors very fast and provides an accurate measurement of oxygen in the lean region.

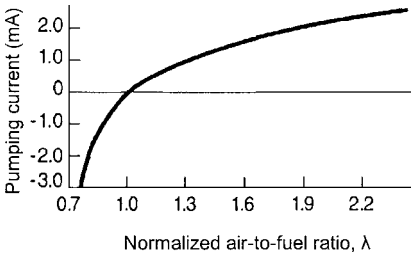

Figure 10 The pumping current characteristic curve of the duel cell amperometric sensor in the rich and lean fuel regions [7].

In determining the response time of these sensors, in addition to the rate of the electrochemical reactions described in Equation 1, the diffusion properties of oxygen and the geometrical parameters of the diffusion barrier also play a role [31]. It is found to vary from fraction of a second to tens of seconds [24]. The oxygen diffusion is generally believed to be the rate determining step in these amperometric sensors. With regard to the long term stability, the thermal cycling of the sensors may change the microstructure and hence the dimension of the porous diffusion barrier, causing drifts in the sensor response.

Garzon *el al.* [32] have studied the suitability of mixed ionic-electronic conducting thin film membranes as dense diffusion barrier. The phenomenon of oxygen diffusion through the thin film due to the oxygen chemical potential gradient from the film surface to the zirconia interface is analogous to the oxygen diffusion through a porous diffusion layer or a diffusion hole. Lanthanum strontium manganate (LSM) is a well studied mixed ionic-electronic conductor for oxygen membranes, and is found to exhibit better diffusion control for the amperometric sensors. Peng *et al.* [33] have demonstrated that a composite of Pt and YSZ may also be used as a diffusion barrier for oxygen concentration below 6% in the test gas. By employing sensors using thick or thin film technology, highly miniaturized versions of amperometric sensors with low power consumption can be realized [34].

Many of the present day fuel economy vehicles use dual-cell amperometric sensors in spite of the higher complexity in packaging and design. With aging, physical modification of the diffusion barrier of the sensor is possible and may cause problems. So, new materials and methods need to be devised in regard to long term durability of the diffusion barriers in the limiting current sensors.

2.3. Semiconducting metal oxide sensors

The semiconducting oxide sensor technology offers advances in new sensor materials, miniaturization and MEMS (micro electronic mechanical system) devices [35]. Basically the electrical properties of most, if not all, of the semiconducting oxides vary with reacting gas species in the atmosphere. Many oxide semiconductors which show good sensitivity to reducing gases like CO, H_2, CH_3, hydrocarbons (HCs) etc. are based on the surface reaction between the sensing material and the gas species [36, 37]. On the other hand, the

TABLE III Carrier, defect type, and sensitivity parameters of semiconducting metal-oxides for oxygen sensing in the temperature range 600–800°C

Semiconductor metal oxides	Carrier type	Defect type	Oxygen sensitivity ($\frac{1}{m}$ in Equation 14)	Ref.
CeO_2	n	$V_{\ddot{O}}$	−5 to −7	[38]
Nb_2O_5	n	$V_{\ddot{O}}$	−4	[39]
$SrTiO_3$[a]	n, p	$V_{\ddot{O}}$,V''_{Sr}	−4 to −6 and 4	[40]
TiO_2	n	$V_{\ddot{O}}$, Ti_{int}	−4 to −6	[41]

[a]Strontium titanate adopts different conduction mechanisms in different P_{O_2} ranges.

bulk defect phenomena are associated with oxygen ion vacancies, metal ion interstitials and vacancies, electrons and holes. Table III lists properties of common semiconducting metal oxides, TiO_2, CeO_2, Nb_2O_5, and $SrTiO_3$ [38–41]. The change in conductance of the material upon exposure to the test gas is due to the change in concentration of oxygen species in the bulk, and is a reflection of the defect structure [36, 42]. The predominant defects in oxide semiconductors are oxygen vacancies and their associated free charge carriers. Oxygen adsorbates are created on the surface of the oxide semiconductor at elevated temperatures by the reaction

$$\frac{1}{2}O_2 + 2e^- + V_{\ddot{O}} \rightarrow O_{ads} \tag{13}$$

A relationship between the oxygen partial pressure and the electrical conductivity of an oxide sensor can be represented by [42, 43]

$$\sigma = A\exp(-E_A/kT)P_{O_2}^m \tag{14}$$

where σ is the electronic conductivity, A is a constant, E_A the activation energy for conduction and m is a parameter determined by both the type of the carrier (n or p) and the defects (e.g., oxygen vacancy) in the semiconductor. For an n-type semiconductor involving oxygen vacancies $V_{\ddot{O}}$, the equilibrium constant for the mass action reaction (Equation 13) is given by

$$K = [V_{\ddot{O}}]n^2\left(P_{O_2}\right)^{\frac{1}{2}} \tag{15}$$

where n is the concentration of electrons. For the charge balance, the concentration of oxygen vacancies $[V_{\ddot{O}}] = n/2$. Then

$$K = \frac{n^3}{2}\left(P_{O_2}\right)^{\frac{1}{2}} \tag{16}$$

Thus, the electron concentration in the conduction band, $n \propto (P_{O_2})^{-\frac{1}{6}}$ i.e., $m = -1/6$. The value of $|m|$ is the sensitivity of the sensor, higher the $|m|$ value, higher the sensitivity and vice versa. Table III lists the m values for a series of semiconducting oxygen sensor materials.

TiO_2 is one of the most widely studied semiconductors for oxygen and other gas sensing applications [2, 44]. It is an n-type semiconductor for a wide range of oxygen partial pressure (P_{O_2}: 1–10^{-30} atm). Since the valence band (filled O-2p states) is nonreceptive to holes and the conduction band (Ti-3d states) is receptive to electrons, the conductivity is due to only the electrons in undoped TiO_2. The crystal structure of TiO_2 (rutile) allows oxygen vacancies $V_{\ddot{O}}$, and titanium interstitials Ti^{4+} or Ti^{3+} to exist in the lattice [45]. So, in addition to reaction (13), other electron contributing reactions involving Ti^{3+} or Ti^{4+} are

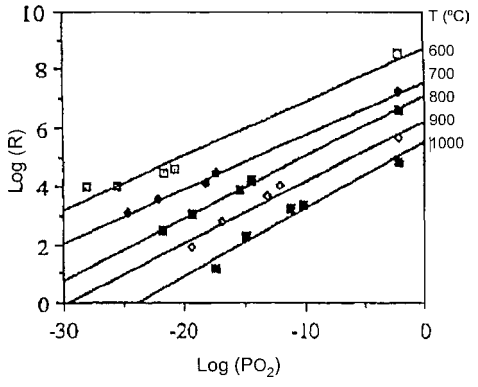

Figure 11 Resistance characteristics of a TiO_2 thin film oxygen sensor in different partial pressure of oxygen [46].

$$TiO_2 \rightarrow Ti_{(int)}^{3+} + 3e^- + O_{2gas} \tag{17}$$

$$TiO_2 \rightarrow Ti_{(int)}^{4+} + 4e^- + O_{2gas} \tag{18}$$

also possible at high temperatures. Then the value of $|m|$, in Equation 14 would be higher than 1/6, due to the mixed conduction mechanisms [45, 46]. Fig. 11 shows the sensing characteristics of a TiO_2 thin film oxygen sensor [46]. It is clearly seen that the resistance of the sensor decreases with decreasing P_{O_2}, the characteristic of an n-type semiconductor. Also for a given temperature, the logarithmic variation of the senor resistance with P_{O_2} is found unaltered for oxygen concentration from 1 to 10^{-30} atm. So, the TiO_2 based oxygen sensor was proposed for controlling the air-to-fuel ratio (λ sensor) in combustion systems [44].

Niobium pentoxide, Nb_2O_5, is another promising material for oxygen sensing. This is an n-type semiconductor with the sensitivity factor of $m = -1/4$ with an activation energy of 1.4 eV for electronic conduction for a P_{O_2} range of 10 ppm to 100% and temperature from 400 to 800°C [39]. The interference from CO, CH_4 and humidity are found to be minimal but the response time is longer (5 min). Doping Nb_2O_5 with acceptor level impurities like TiO_2 decreases the sensitivity factor, $m = -1/5$, but also decreases the activation energy E_A to 0.195 eV [47]. To design sensors stable against fluctuating temperatures, lowering the activation energy leads to higher stability.

Strontium titanate, $SrTiO_3$, belonging to perovskites has been used for oxygen sensor applications. The perovskite structure is stable up to a temperature of 1400°C and dopants can be incorporated without phase transformations. $SrTiO_3$ behaves like an n-type semiconductor in the oxygen partial pressure below 10^{-5} atm (1 Pa) and at higher P_{O_2}, it is a p-type semiconductor with the oxygen sensitivity factor $m = \pm 1/4$ at 800°C [40]. The oxygen vacancies in the n-type

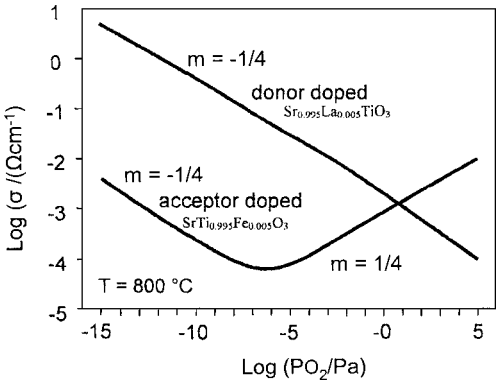

Figure 12 Conductivity variation with oxygen partial pressure in donor doped and acceptor doped strontium titanate. (donor: 0.5 at.% La, acceptor: 0.5 at.% Fe) [48].

region and the strontium vacancies in the *p*-type region contribute to the conductivity in $SrTiO_3$. So, the donor or acceptor impurities can shift the *n*-*p* transition towards either high or low P_{O_2} regions, respectively. Fig. 12 shows the characteristic curves of conductivity variation with oxygen partial pressure in La (donor) and Fe (acceptor) doped $SrTiO_3$ [48]. Lanthanum doped $SrTiO_3$ exhibits the *n*-type conduction throughout the P_{O_2} region. For iron doped samples, the conductivity in the *p*-type region is found to be independent of temperature, i.e., the activation energy E_A is close to zero as seen in Fig. 13, which shows the conductivity variation with P_{O_2} for different concentrations ($x = 0.01$ and 0.35) of the dopant iron.

The response time of the semiconducting sensors is found to be dependant on the materials used and the processing conditions. One of the potential materials being investigated for faster oxygen response is the *n*-type semiconductor, cerium oxide, CeO_2. It has a fluorite structure with a high diffusion coefficient of oxygen vacancies about 10^{-5} cm^2 s^{-1} at 970°C [38, 49]. The fast diffusing oxygen vacancies determine the sensor kinetics at high temperatures and particle size '*d*' of the polycrystalline CeO_2 influences the response time. Izu *et al*. [50] have observed a 10 times faster response (≈8 s) in 200 nm particles compared to 2 μm sized CeO_2 particles as shown in Fig. 14. When the

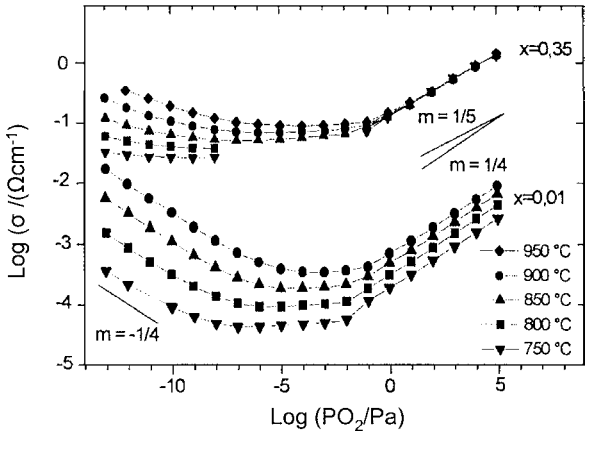

Figure 13 Conductivity as a function of oxygen partial pressure and temperature in $Sr(Ti_{1-x}Fe_x)O_3$ with $x = 0.01$ and 0.35 [48].

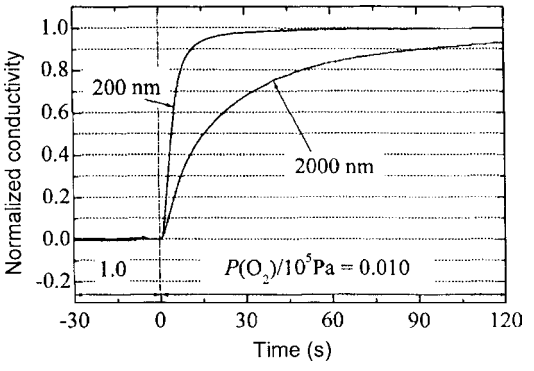

Figure 14 Comparison of response times of CeO_2 oxygen sensor having particle size 200 nm and 2000 nm for the change of P_{O_2} from 105 to 103 Pa at 712°C [51].

particle size is above 1 μm, the kinetics is mainly controlled by surface reaction and is proportional to '*d*' and when the particle size is in the nanometer range, the kinetics is controlled by the diffusion of oxygen vacancies and varies with 'd^2'. The response time is further decreased by dispersing platinum nanoparticles along with that of CeO_2 [51]. The Schottky junctions between the CeO_2 and Pt particles lead to electron transfer from Pt to CeO_2 semiconducting particles which decreases the energy required for oxygen vacancy creation in the lattice. This causes the reduction in response time.

Though oxygen sensors based on semiconducting metal oxides are not extensively used in automobile applications, the discovery of materials with promising characteristics and optimization of methods should lead to miniaturized sensor applications.

2.4. Future trends

Ever since 1970, when the automotive exhaust gas regulations were adopted in USA and subsequently in Japan and Europe, the demand for oxygen sensors has been growing every year as the regulations become more and more stringent. Table IV shows the evolution of oxygen sensor technology since 1976 for use in automobiles [52–54]. The major oxygen sensor manufacturers include: (1) NGK Spark Plug Co. Ltd, Japan, (2) Robert Bosch GmbH, Germany, (3) Delphi Automotive Systems, USA, (4) Denso Corp., Japan, and (5) U-Jecs, Japan. The demand of oxygen sensors in USA from 1996 to 2000 was about 40 million every year, in Europe, it increased from 12 million in 1996 to 25 million in 2002, and in Japan, 6.6 million in 1994 and 7.3 million in 1997 followed by a steady growth [52]. Though the sensors demand is considered saturated in USA and Europe, as other countries also start to follow exhaust emission regulations, the worldwide demand for oxygen sensors is expected to be growing. On the other hand, for satisfying the 'zero emission vehicles' ZEV regulation, oxygen micro-sensors with better performance, e.g., faster response and light-off times, should be developed.

3. Room temperature oxygen sensors

Medical, soil aeration, plant respiration, waste management and food packaging industries [23, 55] have

TABLE IV Evolution of oxygen sensors in the automobile industry [52–54]

Year (Company)	Sensor type	Features	Applications/Market
1976 (Bosch)	Thimble YSZ based potentiometric sensor	Operation temperature relied on the exhaust temperature; light-off time >1 min.	First use in Volvo vehicles as air/fuel—λ sensor
1982 (Bosch)	Heated thimble type YSZ based potentiometric sensor	Separate heater controlled operation; light off time ∼30 s.	λ sensor in many of the vehicles. Nearly 33 million sensors are produced every year by Bosch
1984 (Toyota-Denso)	YSZ based limiting current amperometric sensor	Best suited for lean-burn engines (λ = 22:1)	In Japan car market
1985 (NGK)	Semiconducting titania thin film sensor	Heater controlled; drift in the sensor signal; poor durability	Used in less than 1% of the O_2 sensor equipped vehicles
1991 (NGK)	Dual cell limiting current amperometric sensor (Universal exhaust gas oxygen sensor-UEGO)	Suitable for the whole range of λ values from stoichiometric point to lean burn conditions	Both in USA and Japan car industries
1997 (Bosch)	Thick film YSZ based planar potentiometric senor	Heater integrated; smaller in size; low thermal mass; light off time ∼10 s.	Being used in nearly 30% of the O_2 sensor equipped vehicles

a different requirement for oxygen sensors, since the oxygen is either dissolved in some media (liquid or solid) or oxygen measurements have to be made under ambient, low temperature conditions. Bio-chemical oxygen demand (BOD) is a parameter widely used for monitoring the fate of bio-degradable organic compounds in water [56]. Polarographic oxygen sensors, the best known of which are the Clark electrodes find extensive applications for measuring dissolved oxygen.

The Clark electrode consists of a sensing platinum electrode (cathode) and a reference silver electrode (anode), and enclosed within an oxygen permeable membrane. At a polarizing voltage of 800 mV, oxygen can be reduced into hydroxide ions resulting in a current that is proportional to the oxygen concentration. The electrode reactions are [57].

Cathode(Pt) reaction:

$$\frac{1}{2}O_2 + 2e^- + H_2O \rightarrow 2OH^-_{electrolyte} \quad (19)$$

Anode(Ag) reaction:

$$2Ag + 2Cl^-_{electrolyte} \rightarrow 2AgCl_{Ag} + 2e^- \quad (20)$$

The main disadvantages of Clark electrodes are (i) consumption of oxygen in the form of OH^- leading to more alkaline nature of the electrolyte and (ii) AgCl coating on the silver anode over time reduces the reaction area and hence the reaction finally stops.

Another class of oxygen sensors exploits the paramagnetic properties of oxygen [3]. The sensor design involves a dumb-bell made of glass spheres filled with nitrogen having a reflecting mirror in the center and suspended in a strong non-uniform magnetic field. When oxygen is introduced into the chamber, it is attracted towards the stronger part of the magnetic field and alters the dumb-bell motion, which is analyzed. It is accurate and interference free but is expensive and can not easily be miniaturized.

Another class of sensors for measuring oxygen at room temperature as well as dissolved oxygen are the optical oxygen sensors [58] and is the focus of this review. Optical oxygen sensors are broadly based on quenching of luminescence of dyes by oxygen [59]. These sensors provide an alternative to the conventional electrodes due to their fast response and minimal reactivity with the analyte (no consumption of O_2).

3.1. Optical oxygen sensors

Typically, on absorption of light at their absorption maxima, dye molecules exhibit long excited state lifetimes and emit radiation at longer wavelengths (fluorescence or phosphorescence). The excited state of the luminescent dye can be quenched by an energy transfer mechanism upon collision with oxygen molecules [60]

$$\text{Fluorescence:} \quad L^* \rightarrow L + h\nu \quad (21)$$

$$\text{Quenching:} \quad L^* + O_2 \rightarrow L + O_2^* \quad (22)$$

As a result, the intensity of luminescence is reduced along with the lifetime and the degree of quenching is proportional to the oxygen concentration.

Fig. 15 shows a schematic diagram of an optical oxygen sensor. The active components of the sensor are the luminescent dye encapsulated in a polymer medium, a light source (commonly a LED or laser) for exciting the dye at a particular wavelength, (550–800 nm) [61], a photodiode to detect the fluorescent radiation and an optical fiber for the transmission of light. The quenching of the luminescence can be characterized by the Stern-Volmer eqn. [62]

$$\frac{I_0}{I} = 1 + K_{SV} \cdot P_{O_2} \quad (23)$$

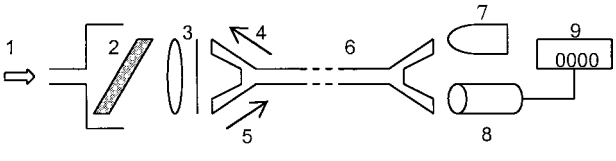

Figure 15 Schematics of an optical oxygen sensor. (1) gas or liquid path, (2) lumophore dispersed on oxygen permeable membrane, (3) lens and filter, (4) exciting radiation, (5) fluoresccent radiation, (6) optical fiber, (7) LED/Laser, (8) photodiode, and (9) display.

where I_0 and I are the luminescent intensities in the absence and presence of oxygen, P_{O_2} in Torr and K_{SV} is the quenching constant which determines the sensitivity of the optical oxygen sensor. K_{SV} is directly proportional to (i) the natural lifetime τ_0 (in the absence of oxygen) of the luminescent excited state, (ii) the oxygen solubility of the quenching medium given by the Henry's constant K_H and (iii) the quenching rate constant k_Q [62] and given by

$$K_{SV} = \tau_0 K_H k_Q / 760 \tag{24}$$

So, the sensitivity of a luminescence based oxygen sensor is influenced by the properties of both the luminescent material and the oxygen permeable encapsulating medium. The natural lifetime of the excited state, τ_0, also depends on the encapsulating medium. However, the increased lifetime of the dye in a given medium may not necessarily be enough for good sensitivity if the oxygen solubility K_H in the medium is poor. In addition, the rate constant of oxygen quenching, k_Q is dependent on the oxygen permeability, P, which is proportional to the diffusion coefficient of oxygen D in the medium. The importance of oxygen diffusion is evident from the observations that the quenching response of fluoranthene dissolved in cyclohexane solution is slower than in a polyethelene film [63]. Also, rapid response and high quenching efficiency have been observed by using porous 'Vycor' glass as the matrix.

Typical luminescent dyes and the polymer matrices used for optical oxygen sensor applications are shown in Table V. The polypyridyl compounds of Ru (II) and metalporphyrins (PtOEP & PdOEP) are the most extensively studied. Structures of various ligands are shown in Fig. 16 [58]. The luminescence character of the Ru(II) metal complexes is described by a charge transfer from ligand to metal. The long lifetimes of the excited states is a reflection of the triplet nature due to the spin-orbit coupling with the metal center [64]. These excited states involve large changes in charge distribution and therefore the spectral properties are strongly influenced by the surrounding medium. Fig. 17 shows the Stern-Volmer plots of oxygen sensitivity I_0/I vs. P_{O_2} for three molecules, $[Ru(bpy)_3]^{2+}$, $[Ru(phen)_3]^{2+}$ and $[Ru(Ph_2phen)_3]^{2+}$ encapsulated in silicone rubber

TABLE V Luminescent dyes and encapsulating polymers for optical oxygen sensors [58, 62–67]

Lumophores	Encapsulating media
Fluoranthene,	Polyethylene
tris(2,2′-bipyridine) ruthenium II $[Ru(bpy)_3]^{2+}$,	Vycor porous glass Silicone rubber (PDMS)
tris(1,10-phenanthroline) ruthenium II $[Ru(phen)_3]^{2+}$,	Silica gel Methanol
tris(4,7-diphenyl-1,10-phenanthroline) ruthenium II $[Ru(Ph2Phen)_3]^{2+}$,	Cellulose acetate butyrate (CAB)
(1,10-phenanthroline) tris (thenoyltrifluoroacetonato) europium III $[Eu(tta)_3\ phen]^{3+}$,	Poly(methylmethacrylate) (PMMA) Poly(vinylchloride)
Platinum Octaethylporphyrin (PtOEP), Palladium Octaethylporphyrin (PdOEP)	Polystyrene

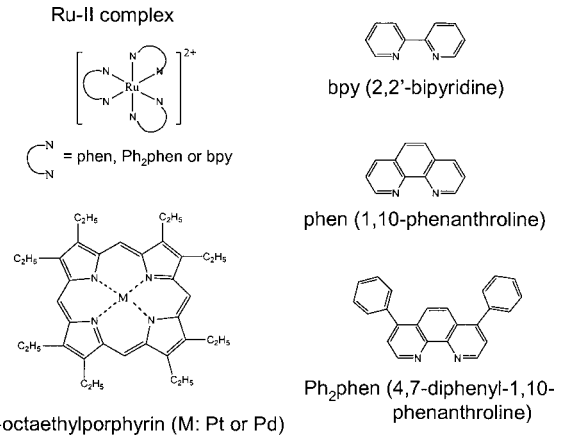

Figure 16 Representative probe molecules used for luminescence based optical oxygen sensors [58].

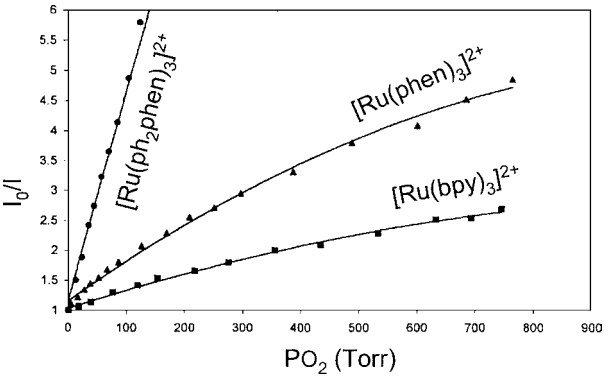

Figure 17 Stern-Volmer plots of I_0/I vs. P_{O_2} for three ruthenium complexes in silicone rubber [62, 64].

[62, 64]. Table VI shows that different lumophores embedded in different polymers exhibit varying sensing characteristics for oxygen [62–66]. Of the popular fluorescent complexes of ruthenium, the lifetime and the sensitivity vary in the order $[Ru(Ph_2phen)_3]^{2+} > [Ru(phen)_3]^{2+} > [Ru(bpy)_3]^{2+}$ as evidenced in the Fig. 17, and the silicone rubber is found to be an efficient polymer medium [62, 64, 65, 67].

One interesting point to note is the downward curvature in the Stern-Volmer (sensitivity) plots as seen in Fig. 17 [68]. This poses problems in calibrating these optical sensors. Though there are models based on theoretical fitting procedures e.g., power law model, two-site model, and Gaussian distribution of τ_0 and k_Q [62, 66, 67, 69], the physical understanding of the nonlinearity is still not adequate. The assumption is that the metal complex is in different environments with different quenching rate constants.

Another important set of dyes is the metal-porphyrin complexes, especially, platinum-octaethylporphyrin (PtOEP) and palladium-octaethylporphyrin (PdOEP) [66]. Due to the increased lifetime of the phosphorescent excited state in these complexes (100 μs–1 ms), the sensitivity is normally larger than the Ru(II) complexes. And also, the larger Stokes shift (difference in the wavelength of the exciting and emitting radiations (>100 nm) makes the measurement easier [70]. The porphyrin based systems exhibit faster response times

TABLE VI Oxygen sensing characteristics of different lumophores embedded in different polymers

Lumophore	Polymer	Natural life-time $\tau_0(\mu s)$	Oxygen sensitivity, K_{SV}	Ref.
Fluoranthene	Vycor glass	–	0.003	[63]
$[Ru(bpy)_3^{2+}(ClO_4^-)_2]$	Silicon rubber-RTV 118	0.62	0.003	[62, 64]
$[Ru(phen)_3^{2+}(ClO_4^-)_2]$	–do–	0.92	0.009	[62, 64]
$[Ru(ph_2phen)_3^{2+}(ClO_4^-)_2]$	–do–	5.3	0.033	[62, 64]
–do–	Poly(acrylic acid)	–	0.0015	[65]
–do–	Poly(sodium 4-styrene sulfonate)	–	0.002	[65]
PtOEP	Ethyl cellulose	81	0.196	[66]
PdOEP	–do–	1410	3.475	[66]

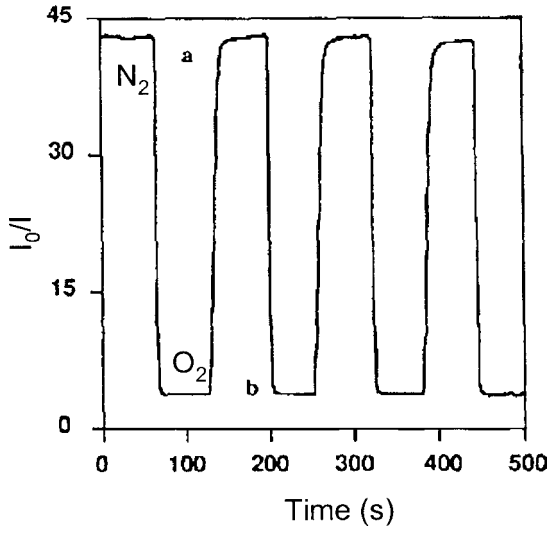

Figure 18 The response time and relative intensity change for PtOEP in silica glass when switching from 100% N_2 to O_2 and back [71].

as compared to the Ru complexes. A typical dynamic response of a PtOEP in silica glass oxygen sensor is shown in Fig. 18. When changing from 100% nitrogen to 100% oxygen, the response time is 5 s and from O_2 to N_2, it is about 10 s. But, the t_{90} is still less than 5 s in both the cases [71].

As far the interference effects from other gases and liquid species are concerned, in both the group of sensors, when hydrophobic medium is used as a matrix, a variety of potential interferents including bleach, cyclopropane, halothane, N_2O, H_2S, CO_2 and humidity are well excluded [67, 72].

While research on optimizing the oxygen sensing characteristics of the luminescent materials is being carried out worldwide, the use of optical oxygen sensors has already emerged. Many municipalities and waste water treatment plants in the USA have started using optical oxygen sensors. Materials and performance optimization of these optical sensors are expected to increase their share of the package waste water market for dissolved oxygen sensors.

Acknowledgement

The authors acknowledge the useful discussions with Nick Szabo and Chonghoon Lee. This work was supported by CISM through NSF grant # EEC-9523358 and NASA-GMI program.

References

1. J. BINDER, *Sensors and Actuators* A **31** (1992) 60.
2. A. M. AZAD, S. A. AKBAR, S. G. MHAISALKAR, L. D. BIRKEFELD and K. S. GOTO, *J. Electrochem. Soc.* **139** (1992) 3690.
3. R. KOCACHE, *Sensor Rev.* **14** (1994) 8.
4. C. B. ALCOCK, *Solid State Ionics* **53–56** (1992) 3.
5. J. W. SCHWANK and M. DIBATTISTA, *MRS Bull.* June (1999) 44.
6. T. TAKEUCHI, *Sensors and Actuators* **14** (1988) 109.
7. J. RIEGEL, H. NEUMANN and H.-M. WIEDENMANN, *Solid State Ionics* **152–153** (2002) 783.
8. N. M. SAMMES, G. A. TOMPETT, H. NÄFE and F. ALDINGER, *J. Euro. Ceram. Soc.* **19** (1999) 1801.
9. M. MOGENSEN, N. M. SAMMES and G. A. TOMPSETT, *Solid State Ionics* **129** (2000) 63.
10. C. XIA and M. LIU, *Adv. Mater.* **14**(7) (2002) 521.
11. N. M. SAMMES and Z. CAI, *Solid State Ionics* **100** (1997) 39.
12. W. C. MASKELL and B. C. H. STEELE, *J. Appl. Electrochem.* **16** (1986) 475.
13. K. NISHIO, in "The Fundamentals of Automotive Engine Control Sensors" (Fontis Media, The Netherlands, 2001).
14. R. RAMAMOORTHY, S. RAMASAMY and D. SUNDARARAMAN, *J. Mater. Res.* **14** (1999) 90.
15. A. MITTERDORFER and L. J. GAUCKLER, *Solid State Ionics* **117** (1999) 187.
16. N. L. ROBERTSON and J. N. MICHAELS, *J. Electrochem. Soc.* **137** (1990) 129.
17. H.-D. WIEMHÖFER, in British Ceramic Proceedings on Ceramic Oxygen Ion Conductors and Their Technological Applications, No. 56, edited by B. C. H. Steele (The Institute of Materials, 1997).
18. E. I. TIFFEE, K. H. HARDTL, W. MENESKLOU and J. RIEGEL, *Electrochim. Acta* **47** (2001) 807.
19. A. G. MOTIMER and G. P. REED, *Sensors and Actuators* B **24/25** (1995) 328.
20. A. K. M. S. CHOWDHRY, S. A. AKBAR and J. R. SCHORR, *J. Electrochem. Soc.* **148**(2) (2001) G91.
21. E. V. SETTEN, T. M. GÜR, D. H. A. BLANK, J. C. BRAVMAN and M. R. BEASLEY, *Rev. Sci. Instr.* **73** (2002) 156.
22. A. D. BRAILSFORD and E. M. LOGOTHETIS, *Sensors and Actuators* B **52** (1998) 195.
23. M. L. HITCHMAN, in "Measurement of Dissolved Oxygen" (John Wiley & Sons, New York, 1978).
24. G. REINHARDT, R. MAYER and M. RÖSCH, *Solid State Ionics* **150** (2002) 79.
25. T. USUI, A. ASADA, M. NAKAZAWA and H. OSANAI, *J. Electrochem. Soc.* **136** (1989) 534.
26. T. USUI, K. NURI, M. NAKAZAWA and H. OSANAI, *Jpn. J. Appl. Phys.* **26** (1987) L2061.
27. W. C. MASKELL, *Solid State Ionics* **134** (2000) 43.
28. M. BENAMMAR, *Meas. Sci. Tech.* **5** (1994) 757.
29. R. C. COPCUTT and W. C. MASKELL, *Solid State Ionics* **53–56** (1992) 119.
30. R. E. HETRICK, W. A. FATE and W. C. VASSELL, *Appl. Phys. Lett.* **38** (1981) 390.
31. P. R. WARBURTON, M. P. PAGANO, R. HOOVER, M. LOGMAN and K. CRYTZER, *Anal. Chem.* **70** (1998) 998.

32. F. GARZON, I. RAISTRICK, E. BROSHA, R. HOULTON and B. W. CHUNG, *Sensors and Actuators* B **50** (1998) 125.
33. Z. PENG, M. LIU and Ed. BALKO, *ibid.* B **72** (2001) 35.
34. S. YU, Q. WU, M. T-. AZAR and C.-C. LIU, *ibid.* B **85** (2002) 212.
35. D. E. WILLIAMS, *ibid.* B **57** (1999) 1.
36. U. LAMPE, M. FLEISCHER, N. REITMEIER and H. MEIXNER, in "Sensors Update," edited by H. Baltes, W. Göpel and J. Hesse (VCH, New York, 1996).
37. Y. XU, X. ZHOU and O. T. SORENSEN, *Sensors and Actuators* B **65** (2000) 2.
38. J. GERBLINGER, W. LOHWASSER, U. LAMPE and H. MEIXNER, *ibid.* B **26–27** (1995) 93.
39. A. KOHLI, C. C. WANG and S. A. AKBAR, *ibid.* B **56** (1999) 121.
40. N.-H. CHAN, R. K. SHARMA and D. M. SMYTH, *J. Electrochem. Soc.* August (1981) 1762.
41. G. SBERVEGLIERI, *Sensors and Actuators* B **23** (1995) 103.
42. P. T. MOSELEY and A. J. CROCKER, "Sensor Materials" (IOP Publishing, Bristol, 1996).
43. P. T. MOSELEY, *Sensors and Actuators* B **6** (1992) 149.
44. A. TAKAMI, *Ceram. Bull.* **67** (1988) 1956.
45. D. M. SMYTH, "The Defect Chemistry of Metal Oxides" (Oxford University Press, New York, 2000).
46. M. LI and Y. CHEN, *Sensors and Actuators* B **32** (1996) 83.
47. J. ZHU, C. REN, G. CHEN, C. YU, J. WU and H. MU, *ibid.* B **32** (1996) 209.
48. W. MENESKLOU, H-J. SCHREINER, K. H. HÄRDTL and E. I. TIFFEE, *ibid.* B **59** (1999) 184.
49. F. MILLOT and P. De MIERRY, *J. Phys. Chem. Solids* **46** (1985) 797.
50. N. IZU, W. SHIN, N. MURAYAMA and S. KANZAKI, *Sensors and Actuators* B **87** (2002) 95.
51. S. V. MANORAMA, N. IZU, W. SHIN, I. MATSUBARA and N. MURAYAMA, *ibid.* **89** (2003) 299.
52. S. SUZUKI, Y. NODA and N. SAWAKI, *Sensors Update* **6**(1) (1999) 381.
53. Y. NODA, S. ISHIKAWA, N. HAYAKAWA, S. KAWARIJI and H. IIMI, in JSAE Spring Convention Proc. 9832017 (1998) p. 101.
54. Bosch Oxygen Sensors: http://www.forparts.com/Bos02update2.htm
55. M. SMIDDY, N. PAPKOVSKAIA, D. B. PAPKOVSKY and J. P. KERRY, *Food Res. Int.* **35** (2002) 577.
56. C. PREININGER, I. KLIMANT and O. S. WOFBEIS, *Anal. Chem.* **66** (1994) 1841.
57. http:/www.eutechinst.com/techtips/tech-tips16.htm
58. X. LU and M. A. WINNIK, *Chem. Mater.* **13** (2001) 3449.
59. C. KOLLE, W. GRUBER, W. TRETTNAK, K. BIEBERNIK, C. DOLEZAL, F. REININGER and P. O. LEARY, *Sensors and Actutors* B **38–39** (1997) 141.
60. B. R. EGGINS, in "Chemical Sensors and Biosensors" (John Wiley & Sons, England, 2002) p. 53.
61. D. G. FRESNADILLO, M. D. MARAZUELA, M. C. M. BONDI and G. ORELLANA, *Langmuir* **15** (1999) 6451.
62. A. MILLS, *Sensors and Actutors* B **51** (1998) 60.
63. I. BERGMAN, *Nature* **218** (1968) 396.
64. E. R. CARRAWAY, J. N. DEMAS, B. A. DEGRAFF and J. R. BACON, *Anal. Chem.* **63** (1991) 337.
65. Y. AMAO and I. OKURA, *Sensors and Actuators* B **88** (2003) 162.
66. P. DOUGLAS and K. EATON, *ibid.* B **82** (2002) 200.
67. J. R. BACON and J. N. DEMAS, *Anal. Chem.* **59** (1987) 2780.
68. H. CHUANG and M. A. ARNOLD, *Anal. Chim. Acta* **368** (1998) 83.
69. A. MILLS, *The Analyst* **124** (1999) 1301.
70. D. B. PAPKOVSKY, *Sensors and Actuators* B **29** (1995) 213.
71. S.-K. LEE and I. OKURA, *The Analyst* **122** (1997) 81.
72. K. EATON and P. DOUGLAS, *Sensors and Actuators* B **82** (2002) 94.

Received 19 May
and accepted 9 July 2003